RADIATION PROPERTIES OF PULSAR MAGNETOSPHERES: OBSERVATION, THEORY, AND EXPERIMENT

KEVIN R. HEALY
Very Large Array Operations Center
National Radio Astronomy Observatory
Socorro, New Mexico, USA

and

ANTHONY L. PERATT
Physics Division
Los Alamos National Laboratory
Los Alamos, New Mexico, USA

Abstract. In the three decades since their discovery, the accumulated body of observational data from pulsar sources puts constraints on models that seek to explain their periodic radiation. This paper reviews this data, reports on a VLA search for haloes predicted by an early model, and reinvestigates a magnetospheric disk–field–aligned–current transmission line system as the origin of the observed radiation, with external wave excitation by as yet an unexplained source. Three dimensional, fully electromagnetic particle–in–cell simulations of the pulsar surface and magnetosphere are used to explore the waveshape and polarization properties of the observed radiation.

Key words: Pulsars, Radio Astronomy, Plasma Astrophysics

1 Introduction

Unexpectedly in 1967, J. Bell and A. Hewish detected a highly stable train of pulses of radio emission from the constellation Vulpecula during an investigation of extragalactic radio sources (Burnell 1983, Backer 1988). This train had a periodicity of 1.337 s.

The low galactic altitudes of this first 'pulsar', and soon thereafter, several other 'pulsars', suggested that these radiation regions were imbedded within our Galaxy. Furthermore, millisecond intensity fluctuations of the radio signals implied that the emitting regions had dimensions less than 300 km.

Because of the stability of the pulse period, Thomas Gold (1968) concluded that pulsars must be highly magnetized, rapidly rotating neutron stars. This model of a pulsar's emission qualitatively describes it as high energy plasma beams emitted from the poles of a spinning neutron star and accelerating along the stars's dipole magnetic field, emitting curvature radiation as pulses towards the observer. In the three decades since their discovery, most new observations have been able to be described in terms of the standard, search-light, model.

Astrophysics and Space Science **227**: 229–253, 1995.

In spite of the successes of the standard model, there yet exists no self-consistent theory to describe the pulsar electrodynamics. The basic radiation mechanism, the acceleration of relativistic electrons along a curvature producing force, is beyond doubt. Nevertheless, how the relativistic electrons beams are produced and why they possess the observed polarizations are major problems any model must answer (Verschuur & Kellerman 1988).

In particular, any model must address the following known pulsar features:

1. Radio luminosities estimated to lie in a range $10^{27} - 10^{30}$erg/s ($10^{20} - 10^{23}$W);
2. Pulse periods within a range of a millisecond to several seconds;
3. Stable mean pulse profile having one, two, or three components;
4. Monotonic rotation of linear polarization vector with a signature that depends on the component structure;
5. Slow decrease of the pulse width with increasing radio frequency, and with increasing period;
6. Slow increase of periodicity, usually with dP/dt in a range between $10^{-14} - 10^{-16}$ sec/sec, but for millisecond pulsars as small as 10^{-19} sec/sec;
7. *Glitches*, a jump-like *decrease* of the period P;
8. Interpulse components midway between the main pulses;
9. A continuum, low-power background;
10. Linear polarization angle modes spaced by 90°;
11. A circularly polarized component that reverses polarity between peaks in the main pulse;
12. Memory in the pulse–to–pulse fluctuations which in some pulsars takes the form of periodically spaced subpulses drifting slowly in time;
13. Erratic pulse–to–pulse amplitude fluctuations;
14. Micropulses within single pulses that are sometimes periodically spaced.

Other problems a model must address include:

15. The extreme bandwidth of radiation observed, in some pulsars from radio frequencies to gamma ray energies;
16. A very high Doppler-interpreted velocity, up to 500 km/s; and finally:
17. The global pulsar system and topology which, for the Crab Nebula, encompasses a fibrous and filamentary region 2×10^{16} m beyond the pulsar; 'wisps', 'jets', and other features symmetrically oriented 10^{15} m beyond the active region (Hester *et al.* 1994).

A number of suggestions have been offered to address many of the seventeen items listed above. For example, the orientation of core and conal components of beam emission regions with respect to the axis of rotation of a neutron star, its magnetic axis, and the location of the observer are postulated to answer items 3, 4, 8, and 10. Naik and Kulkarni (1994) suggest the existence of field–aligned currents and utilize the Carlqvist Relation (Peratt 1992a) to explain item 9.

A fundamental problem in any pulsar model, the actual emission mechanism for relativistic charged particle beams, is investigated in some detail by Beskin *et al.* (1993). They describe the generation of electron-positron plasma with relativistic parameter $\gamma \geq 10^6 - 10^7$ in a relativistic double layer ($V_{||} \approx 10^{12} - 10^{13}$V) between the surface of the neutron star and its magnetosphere.

Glitches, item 7, once described entirely in terms of 'starquakes,' has more recently been attributed to fluid motions within a stellar core.

Several radiation loss mechanisms have been suggested for Item 6. For example, gravitational quadrapole radiation had been cited as a cause for periodicity lengthening. However, the discovery of millisecond pulsars do not show a decay consistent with this theory (Backer *et al.*).

The content of this paper is ordered as follows. In Section 2 we describe the historical search for pulsar haloes predicted by the standard model that led to the writing of this paper. In Section 3 we report current results with VLA observations of halo-candidate pulsars PSR0809+74, PSR0942-13, and PSR0950+08. Section 4 is a reexamination of the disk-magnetosphere model and a theory of radio emission in a magnetospheric transmission line model. Section 5 reports the measured properties of pulses in a model magnetosphere experimental setup. We present our conclusions in Section 6.

2 The Search for Haloes

In the standard model, what a beam of plasma does after it has left the inner part of the magnetic field is not commonly described in the literature. For example, if the plasma leaves the pulsar system and interacts with the interstellar medium (ISM), the effects of the interaction might be visible to telescopes on Earth.

Twenty years ago, Blandford *et al.* proposed a theory of 'ghost remnants' surrounding old pulsars. While considerable effort has been spent trying to confirm or refute this theory, little progress has been made. Today, the original Blandford theory is outdated, but the observational search for pulsar–related nebulae continues. Past observations of ancient pulsars above 1 GHz have had no success, while searches below 1 GHz have had detections. Recent detections by the Very Large Array and optical observatories of 'pulsar wind nebulae' around fast–moving pulsars have shown the detectability of pulsar wind/interstellar medium interactions. Further possibilities have been opened by recent Hubble Space Telescope observations of the Crab pulsar.

Observations made after Blandford *et al.* (1973) have disproved the swept–shell model, but relativistic pulsar winds as a driving mechanism in the formation of pulsar synchrotron nebulae is still a popular notion. The interpretation of the 'pulsar wind nebulae' is a bow shock formed by ram–

pressure enhanced pulsar wind (Frail and Kulkarni, 1991), while the optical haloes seen around the Crab pulsar have a very striking symmetry related to the pulsar's beams of relativistic particles (J. J. Hester, 1994).

The original theory of Blandford *et al.* (1973) describes a radio halo in terms of a relativistic wind blowing away from the pulsar and interacting with the ISM. This wind would travel through the medium surrounding the pulsar at velocities faster than the Alfvén speed in the medium, expelling the medium and the ambient magnetic field outward. Balancing the flux of the rotational energy lost by the pulsar with the pressure of the interstellar medium provides a way to predict the size of the halo. That is,

$$\frac{\dot{E}_R}{12\pi R^2 V_A} \sim p_{ism}$$

where $\dot{E}_R$ is the rotational energy loss rate, R is the radius of the wind/ISM boundary at equilibrium, V_A is the Alfvén speed in the ISM, and p_{ism} is the pressure of the interstellar medium. For the values provided in Blandford *et al.* (1973) of $\dot{E}_R \sim 10^{32}$ erg s^{-1}, $V_A \sim 10$ km s^{-1} (for $n_e \sim 1$ cm^{-3}, $B \sim 5 \times 10^{-6}$ Gauss), and $p_{ism} \sim 10^{-12}$ dyne cm^{-2}, this gives a value for R $\sim$ 1 pc (see Figure 1a). A halo this size would form in $T \sim R/V_A \sim 10^5$ years. This time is much greater than the age of a supernova remnant, so a halo could easily be distinguished from the original remnant (Blandford *et al.*, 1973).

However, the reports of the first positive detections of a halo around PSR 0950+08 (Gopal–Krishna 1978, Glushak, Pynzar, and Udal'tsov 1981) stated that the object was ~1 arcmin (1') across, only 0.04 pc (8000 AU) in diameter. Even taking into account the modern value of $\dot{E}_R$ for PSR0950+08 is closer to 10^{30} erg s^{-1}, this only lowers the expected diameter of the halo to ~0.1 pc. Obviously another mechanism is at work here, for the wind must be confined by a pressure 10^4 times higher than the pressure of the interstellar medium (see Figure 1b).

2.1 Past Observations

Although the first detection of a possible pulsar radio halo was seen around PSR1919+21, the case for a halo around PSR0950+08 is stronger. It is now thought that PSR1919+21, a pulsar with a proper motion of ~200 km s^{-1}, is superimposed on a more distant supernova remnant, while there appears to be no confusing source behind PSR0950+08.

Shortly after Blandford *et al.* (1973), Weiler, Goss and Schwarz reported on observations done at the Westerbork Radio Synthesis Telescope at 1415 MHz. The purpose of their observations was two–fold: to search for new supernova remnants in the vicinity of known pulsars, and to search for pulsar 'ghosts', the newly theorized haloes.

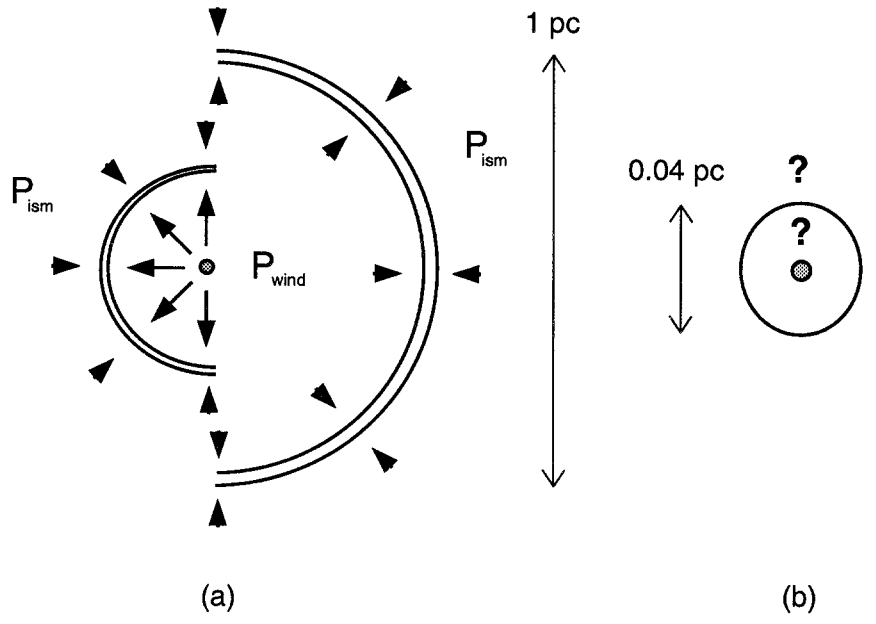

Fig. 1. (a) The Blandford *et al.* model describes a pulsar halo as the interaction of the pulsar's relativistic wind and the interstellar medium, (b) The revised model is still under construction.

To the sensitivity of Westerbork, no supernova remnants or haloes were seen (Weiler, Goss, and Schwarz, 1974). But in light of the later measurements of the size of the PSR0950+08 halo (1' in diameter) and the synthesized beamwidth of the Westerbork array (23 × 196 arcsec in the PSR0950+08 field), it is unlikely that the unpulsed halo emission could have been resolved as seperate from the pulsar's emission.

In 1973 and 1978, Gopal-Krishna, using the proximity of PSR0950+08 to the ecliptic, observed the pulsar during two lunar occultations to search for unpulsed emission. He collected four scans of the pulsar, two immersions and two emersions, each with a different position angle, using the Ooty radio telescope at 327.5 MHz. Analyzing the immersion data from the 1973 occultation and the emersion data from the 1978 occultation seperately, Gopal-Krishna saw evidence of a "halo of continuous emission" with a flux density of 0.2±0.07 Jy at 327.5 MHz and a size of ~1' (Gopal-Krishna, 1978). In addition, he used the null detection of a halo around PSR0950+08 by Schönhardt (1973) at 2.7 GHz to determine a spectral index, α, (the flux,

S, at frequency, ν, is given by $S \propto \nu^{\alpha}$) for the halo observed. His value of a steep index, -0.6, agreed well with the synchrotron emission model for haloes (Gopal–Krishna, 1978). The next report of a positive detection of a radio halo came to a similar conclusion.

Four years later, Glushak, Pynzar', and Udal'tsov reported that they had confirmed a halo around PSR0950+08. Their observations were made at 102.5 MHz with two different telescopes at Pushchino. The BSA, a multi-beam meridional telescope, and the BRT, a interferometer using the BSA and the DKR–1000 telescope, had resolutions of 35' and 16', respectively, in the PSR0950+08 field (Glushak, Pynzar, and Udal'tsov, 1981).

After observing their candidates several times, Glushak, Pynzar', and Udal'tsov found that the PSR0950+08 halo had a 102.5 MHz flux of 2 ± 1 Jy. Using past positive and null detections of the halo, they determined the spectral average for the emission to be -2 ± 1, which was in good agreement with Gopal–Krishna's value (Glushak, Pynzar, and Udal'tsov, 1981).

2.2 Wind Nebulae and Optical Nebulae

Glushak, Pynzar', and Udal'tsov also predicted that high–velocity pulsars would have no visible haloes because the pulsar's relativistic wind would be dispersed over the path of the pulsar, keeping the local injection rate low (Glushak, Pynzar, and Udal'tsov, 1981). In this, they were half right; synchrotron haloes have been seen near fast pulsars only in x–rays to date, but Hα– and radio–emitting shocks have also been detected (Kulkarni and Hester 1988, Frail and Kulkarni 1991, and Cordes, Romani, and Lundgren 1993). These three shock detections all fall into a loose catagory known as 'pulsar wind nebulae'.

Two other observations appear to fall into another catagory of shock–powered structures around relatively slow pulsars. A Very Large Array observation of the Vela pulsar has been made to detect a standing shock in the pulsar's relativistic wind. This 'wisp' is believed to be part of a toroidal shock formed by the pulsar's wind interacting with the interior of the Vela supernova remnant (see Figure 2a) (Bietenholz, Frail and Hankins, 1991). A recent Hubble Space Telescope image of the vicinity of the Crab pulsar shows a pair of circular haloes concentric with what is interpreted as the pulsar's spin axis. These haloes are then thought to be some type of interaction of the pulsar's relativistic beams of particles with the circumstellar medium (J. J. Hester, 1994).

3 VLA Observations of PSR0809+74, PSR0942-13, and PSR0950+08

In March 1993, T. H. Hankins of NRAO and one of the authors, K. R. Healy, observed three nearby pulsars with the VLA at 327.5 MHz. We used a real-

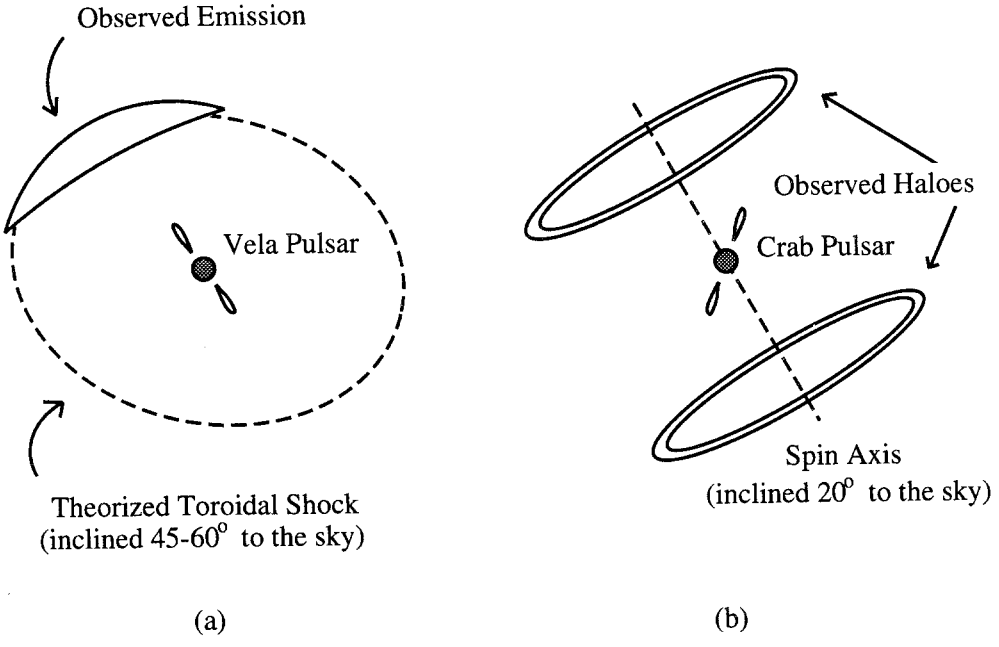

Fig. 2. (a) The 'wisp' detected by Bietenholz, Frail, and Hankins is thought to be part of a larger toroidal shock, (b) while the haloes seen by Hester *et al.* are thought to be the interaction of the pulsar's relativistic particle beams with the circumstellar medium.

time gating system which T. H. Hankins had developed to study pulsars with high time–resolution. The system can produce high time–resolution pulse profiles of pulsars and can split the incoming pulsar signal synchronously with the pulsar's period into two signals; the 'on–pulse' emission and the 'off–pulse' emission. This approach had been successfully used by Bietenholz, Frail and Hankins in 1991 to produce the very high dynamic range maps of the wisp near the Vela pulsar (Bietenholz, Frail and Hankins, 1991). We hoped to use this filtering technique to remove the bright pulsar from the data and make high sensitivity maps of the area around our three targets.

Our targets were selected on several criteria. Our first choice was PSR0950 +08, the target source for Gopal–Krishna's occultation experiment, and the Glushak, Pynzar', and Udal'tsov positive detection. From this candidate, we determined our selection criteria to find other pulsars with similar properties. PSR0950+08 is relatively stationary in space, with a transverse velocity of $\sim$15 km s^{-1}, and it is very nearby, 130 pc. It also appears to be a fairly ancient pulsar, having an energy loss rate of $\sim 10^{32.75}$ erg s^{-1}, well below the

canonical $\dot{E}_R$ of 10^{36} erg s^{-1} for the newest pulsars. The properties of our other candidates are summarized in Table I.

TABLE I
Properties of VLA Pulsar Halo Search Candidates

1950 Name	Period (s)	Distance (pc)	v_t (km s^{-1})	$\log(\dot{E}_R)$ (erg s^{-1})
PSR0809+74	1.29224	320	41	30.49
PSR0942−13	0.57026	710	48	31.00
PSR0950+08	0.25307	130	15	32.75

Each of these pulsars was observed in B Array (beamwidth of 15") in Phased Array Spectral Line mode for one hour. This allows a theoretical noise level for the map of 1 Jy/beam. In addition, the Phased Array was required to ensure all antenna signals would arrive at the gating system in phase, and Spectral Line mode was used to allow data that were corrupted by terrestrial interference to be removed.

A very clean map of PSR0809+74 shows no evidence of structure like that seen by Gopal–Krishna; maps of the other two pulsars are noiser and are currently being further processed.

We now turn to the task of modeling a pulsar. Our research is divided into three tasks: i) the total pulsar system and environment, with dimensions reaching 10^{16} m, ii) the pulsar magnetosphere, whose dimensions may be of order 10^8 m, and iii) the active radiation region, whose dimensions may range from hundreds of kilometers to 10^7 m. The remainder of this paper deals only with the pulsar magnetosphere.

4 Magnetospheric Transmission Line Model

Michel and Dessler (Michel & Dessler, 1981; Michel, 1982) suggested the presence of a fossil disk in all pulsars. The purpose of the disk hypothesis was to solve a problem concerning the balance of charges in a corotating magnetosphere. It was soon found that one of the other attributes of a disk was a realistic mechanism for increasing P. For example, in the Michel-Dessler model, the rate of energy loss varies as P^{-3}. This was consistent with the slow rate of energy loss by millisecond pulsars in the presence of a smaller magnetic field, when these were discovered.

If the disk consists of matter in the plasma state, then it is likely that this material is electromagnetically coupled to the magnetosphere via field-aligned currents. To model this coupling, we employ a transmission line mod-

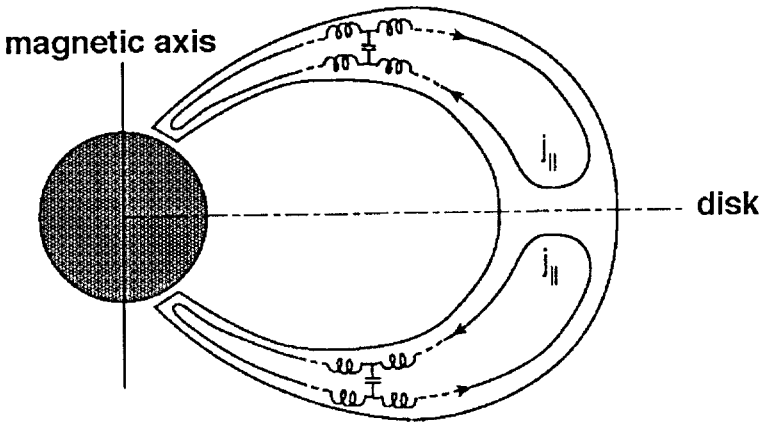

Fig. 3. Transmission line model for magnetic field-aligned currents in a magnetospheric plasma configuration. The north and south pole transmission lines need not be symmetric. The disk may lie between the north and south pole currents, on the equator, or may extend to higher latitudes.

el similiar to that used to describe planetary magnetospheres (Sato 1987)[1]. Figure 3 illustrates a magnetospheric transmission line model for field-aligned currents $j_{||}$ that couples a source region to a load (radiation) region.

The following sections investigate the properties of synchrotron radiating, field-aligned current pulses propagating in a pulsar's magnetosphere.

4.1 Characteristics of a Transmission–Line Pulse

Any disturbance on a transmission line, such as an arc-discharge or an interruption of steady-state conditions, results in the initiation of traveling waves, which propagate towards the ends of the line, where they may be reflected

[1] The similarity between the pulsar phenomenon and the Jovian decametric emissions were noted almost immediately (Michel 1982). Jovian decametric bursts originate from relativistic electrons ($\sim$ 30 MeV; comparable to the 170 MeV pole–to–equator potential drop) spiralling around Jupiter's dipole magnetic field ($\sim$ 4 G) and in the Io-Jupiter flux tube, not from planetary-satellite rotation. The highest (decametric) frequencies come from regions closest to the planet while the lower (kilometric) frequencies are emitted much farther away.

and modified, and attenuated and distorted by any losses until they die out.

The mathematical description of the pair of voltage ϕ and current i traveling waves, along direction z, are given by :

$$\begin{aligned} \phi(z,t) &= \phi^+(z-ut) + \phi^-(z+ut) \\ i(z,t) &= \tfrac{1}{Z_c}\left[\phi^+(z-ut) - \phi^-(z+ut)\right] \end{aligned} \tag{1}$$

where $Z_c = (L/C)^{1/2}$ is the characteristic impedance of a transmission line with inductance L and capacitance C, and $u = (LC)^{-1/2}$ is the propagation constant of the line. The left and right traveling voltage components are (Peratt 1992b):

$$\begin{aligned} \phi^+ &= \tfrac{Z_c}{Z_g+Z_c} \sum_{n=0}^{\infty} \Gamma_g^n \Gamma_l^n \phi\left\{t - \tfrac{1}{u}\left[z + 2l\ n\right]\right\} \\ \phi^- &= \tfrac{Z_c}{Z_g+Z_c} \sum_{n=0}^{\infty} \Gamma_g^n \Gamma_l^{n+1} \phi\left\{t - \tfrac{1}{u}\left[-z + 2l\ (n+1)\right]\right\} \end{aligned} \tag{2}$$

The voltage reflection coefficients are:

$$\Gamma_g = \frac{Z_g - Z_c}{Z_g + Z_c},\ \Gamma_l = \frac{Z_l - Z_c}{Z_l + Z_c} \tag{3}$$

for line surface and disk resistances Z_g and Z_l, respectively.

Consider now a particular case of a lossless 0.4 Ω impedance transmission line of length $l = 10^8$ m (Peratt 1992c). We launch a 20 ms, 10^{13-16}V voltage pulse ($\gamma = 2 \times 10^{7-10}$) from the surface. [Either surface or disk launching is permissible; both lead to the same result]. This voltage is a value associated with relativistic double layers (Peratt 1992d). We suppose that highly ionized plasma of high conductivity terminates both ends of the line so that, to first approximation, $Z_g = Z_l = 0$ and $\Gamma_g = \Gamma_l = -1$. On a lossless line with perfect end conductors the pulses propagate back and forth, forever. In reality, kinetic energy of the relativistic currents flowing along the guide magnetic field is lost in synchrotron radiation.

It is of interest to measure the currents and voltages in the line near the surface, where the current curvature is strongest. These waveforms are shown in Figure 4 for probes located 3×10^5 m (300 km) and 10×10^6 m (10^4 km), respectively, from the surface. As shown, after time 0, each waveform consists of two components, an incident (left-traveling) wave and a reflected (right-traveling) wave. Together, these produce the following features seen in more detail in Figure 5:

- Either a double-hump or single-hump current profile with periodicity 0.65 s;
- A concomitant voltage pulse that reverses polarity over the current profile;

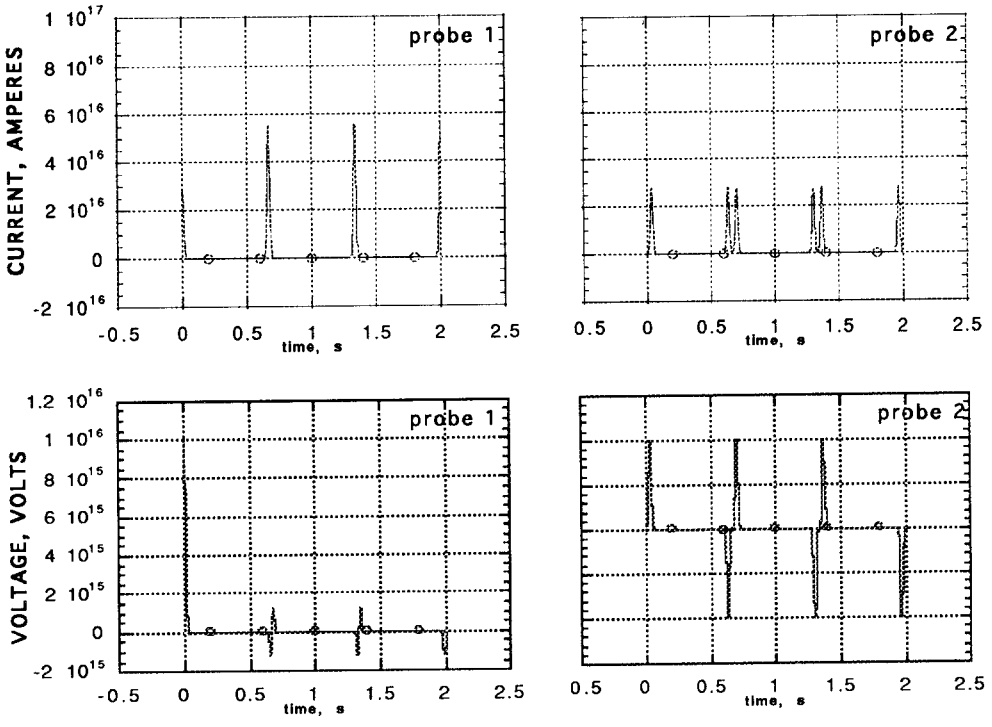

Fig. 4. Current and voltage pulses near the pulsar surface. (top) Current pulses at 3×10^5m and 10×10^6m. (bottom) Voltage pulses.

The relativistic 10^{13-16} A current flowing at the surface is thought responsible for the pulsar emission. The spatial extent of the current is determined by the depth to which the incident wave propagates. This, in turn, is determined by the response of the lower pulsar magnetosphere to an incident broad-band electromagnetic pulse. The problem then turns to the analysis of electromagnetic waves incident on a bounded plasma or wave resonator region (Lysak, 1993; Thompson & Lysak, 1995).

Figure 6 illustrates the electromagnetic waves associated with traveling waves on a transmission line. Depending on how the transmission line intersects the conducting surface or lower magnetosphere, either **E** or **B** may be perpendicular to the plane of incidence. In either case, the reflected electric field is 180° out of phase with the incident electric field. [The change in polarity of the voltage pulses in Figure 5 means that the electric field also reverses polarity].

By convention, the relativistic electrons flow in a direction opposite to that of the high-γ current, and the radiation is beamed in the direction of electron propagation. This direction remains unchanged at the plane of

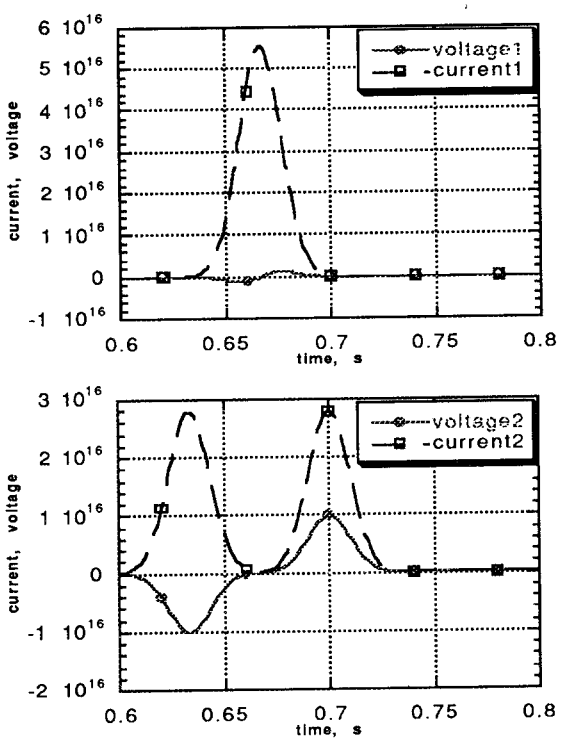

Fig. 5. Magnified current and voltage pulses from figure 4 at (top) 3×10^5m, (bottom) 10×10^6m.

incidence but the field polarization changes by 180°. This is observation is consistent with D and S_t class pulsars that show either a double or single pulse, but a polarization change across the entire pulse profile.

The property of total reflection has been used to produce circularly polarized waves. If the incident wave is linearly polarized in a direction which is neither parallel to nor perpendicular to the plane of incidence, the reflected wave is, in general, elliptically polarized. The degree of circular/elliptical polarization in pulsars can be 10–30% of the total intensity in pulsars. It is signficant that the circular component changes polarity at the maximum of a S_t pulse, characteristic of an oblique reflection off a conducting surface.

The reflection coefficient R for the field is:

$$R \approx \frac{\cos\theta - \frac{1}{2}(1+i)\,\gamma_\omega}{\cos\theta + \frac{1}{2}(1+i)\,\gamma_\omega} \tag{4}$$

where $\gamma_\omega = \sqrt{2\omega\varepsilon_1\mu_2/\mu_1\sigma_2}$.

At the interface $E = (1 + R)$ and the properties of the emitted radiation are frequency dependent. Any pulse component at frequency ω prop-

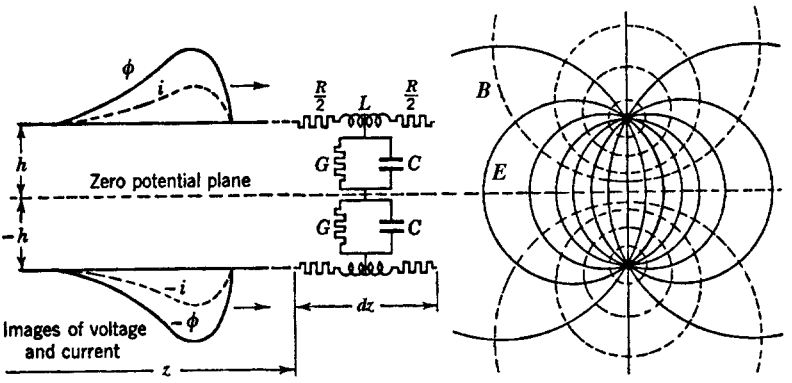

Fig. 6. Traveling waves $\phi(z,t)$ and $i(z,t)$ on a transmission line and associated electromagnetic fields **E** and **B**. The parameters L, C, R, and G are the self-inductance, capacitance, resistance, and transverse conductance, per unit length, respectively. The electromagnetic fields shown are those for a two-filament transmission line (intense field-aligned sheet currents generally undergo filamentation into current strands).

agates with spatial dependency $\exp(-z/\lambda_E)$ to the *collisionless skin depth*, $\lambda_E = c/\sqrt{\omega_{pe}^2 - \omega^2}$, where c is the speed of light and ω_{pe} is the angular plasma frequency. Therefore, in order to calculate the collisionless skin depth, some estimate must be made regarding the lower magnetosphere density and distribution.

Regardless of density profile, if $\omega >> \omega_{pe}$, λ_E is imaginary and the wave propagates freely. Hence, high frequencies propagate freely until a reflection condition $\omega = \omega_{pe}$ is encountered. The radiating currents are thin surface currents.

For frequencies $\omega << \omega_{pe}$, $\lambda_E \approx c/\omega_{pe}$ and the current may be spatially distributed over great distances within the magnetosphere. Table II lists collisionless skin depth versus plasma density for a number of cosmic plasmas.

For the readers convenience, we list some electromagnetic frequency/wavelength bands in Table III. Comparison of λ_E to λ shows that the extent of

TABLE II
Collisionless Skin Depths Versus Plasma Density

Plasma	Density, cm^{-3}	λ_E
stellar wind	0.1	16.8 km
current sheet (Earth)	1	5.3 km
magnetosheath	5	2.4 km
solar corona	10^7	1.68 m
solar surface	10^{15}	0.168 mm
solar center	10^{26}	0.53 nm

the emission region may be extreme depending on frequency of observation.

TABLE III
Electromagnetic Frequency/Wavelength Bands

Band	f-lower	f-upper	λ-lower	λ-upper
MF	300 kHz	3 MHz	100 m	1 km
HF	3 MHz	30 MHz	10 m	100 m
VHF	30 MHz	300 MHz	1 m	10 m
UHF	300 MHz	3 GHz	10 cm	1 m
SHF	3 GHz	30 GHz	1 cm	10 cm
EHF	30 MHz	300 GHz	1 mm	1 cm
Submillimeter	300 GHz	3 THz	100 μm	1 mm
Infrared	3 THz	430 THz	700 nm	100 μm
Visible	430 THz	750 THz	400 nm	700 nm
Ultraviolet	750 THz	30 PHz	10 nm	400 nm
X Ray	30 PHz	3 EHz	100 pm	10 nm
Gamma Ray	3 EHz			100 pm

4.2 Simulation of Pulses in a Magnetospheric transmission Line

We choose to simulate the pulse carrying magnetosphere with a three-dimensional particle-in-cell model. This approach allows us to:

- Insert dipole magnetic fields and double layer electric fields along the line.

- Investigate the pulse characteristics over a wide range of frequencies. For example PSR 0531+21 (Crab) is observed from radio frequencies (430 MHz) to gamma ray energies (greater than 50 MeV).
- Include surface and line curvature and associated field gradients.
- Include nonuniform plasma densities.
- View directly the relativistic currents in the high-curvature, synchrotron emitting regions.
- Investigate glitches when high voltages cause particle leakages across the line.

Figure 7 illustrates the geometry at hand. Field-aligned current pulses propagate at high latitude along the dipole magnetic field. Two regions of high-density plasma terminate this magnetospheric transmission line: plasma near the pulsar surface and plasma at the disk. The transmission line may also contain another active element, a double layer, whose field orientation is also depicted in Figure 7. This figure is axially symmetric about the magnetic axis so that the complete figure of revolution is a torus and the relativistic current pulses propagate within a toroid waveguide. The emission region is a cone of radiation centered on the magnetic axis. No other constraints are placed upon the orientation or rotation of the model; the observer need only be looking in the direction of the instantaneous velocity of the relativistic electrons.

The pulsar magnetosphere transmission line is modelled by two current conducting boundaries that represent the inward and outward field-aligned currents. These boundaries should generally follow a dipole magnetic field profile but, in the simulation model are simply taken to be coaxial. Thus the waveguide geometry is cylindrical in the (z,r,θ) coordinate frame. The line is terminated by two conductors: the pulsar surface and disk. In this scoping study both conductivities are set to $\sigma = \infty$. In reality, cosmic plasmas have finite conductivities that are frequency dependent.

Again, a voltage pulse is launched from the pulsar surface along a line of arbitrary length 100. [Either disk or surface launching of waves is permissible in the simulation]. To measure the electrical constituitive parameters within the line, we place clusters of probes along the transmission line.

Figure 8 shows contours of the propagating radial E_r field at arbitrary computer times 200 (traveling leftwards towards the surface) and 280 (propagating rightwards after reflecting off the surface). Because of the conducting boundary, the polarity of E_r has reversed 180° while the polarization of the azimuthal magnetic field B_θ remains the same (Figure 9).

The simulation analog of Figure 5, the time histories of current and voltage probes placed within the high curvature region, are shown in Figure 10. We

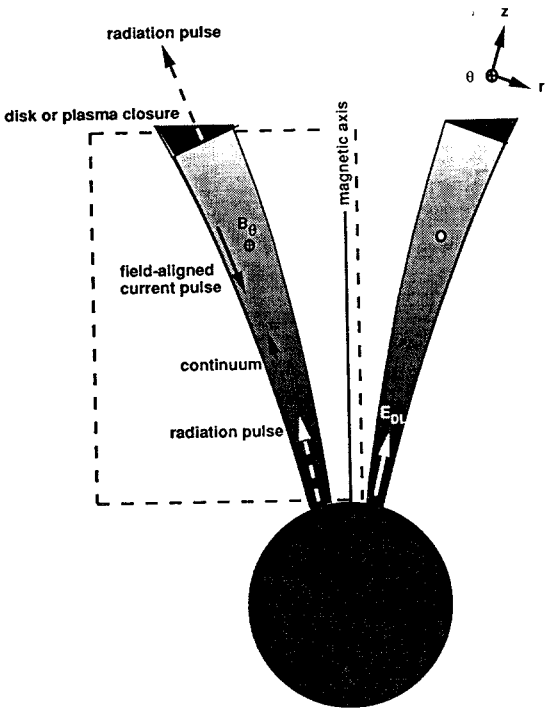

Fig. 7. Simulation geometry. Relativistic current pulses propagate along the dipole magnetic field lines at high latitude and are reflected off high-density plasma near the pulsar surface and magnetosphere disk. The disk may be either located at the equator (long transmission line case) or, as in this figure, at a higher latitude (short transmission line case). The figure is axially symmetric about the magnetic axis and forms a toroidal waveguide. Three emission regions are shown: near the surface, at the disk, and a continuum along the entire transmission line. The dashed–box outlines the simulation region.

again measure either a single or double pulse profile. Figures 8, 9, and 10 pertain to a relativistic pulse traveling on a transmission line in the absence of plasma. When plasma is allowed to flow between the current boundaries a number of important modifications are observed in the simulated waveforms.

As the electric field propagates along the line (e.g., Figure 8), electrons accelerate away from the boundary in the $-E_r$ direction. However, because of the intense B_θ field associated with the current pulse (Figure 7), they are constrained to flow along the boundary in $\mathbf{E} \times \mathbf{B}$ drift rather than across the line.

When scaled to magnetosphere transmission line dimensions, the entire 10^8 m line acts a continuous source of of low-level radiation and noise. [All pulsars show background radiation, *i.e.*, noise between the pulses with amplitudes between several millijansky to a few hundreds of mjy. For example,

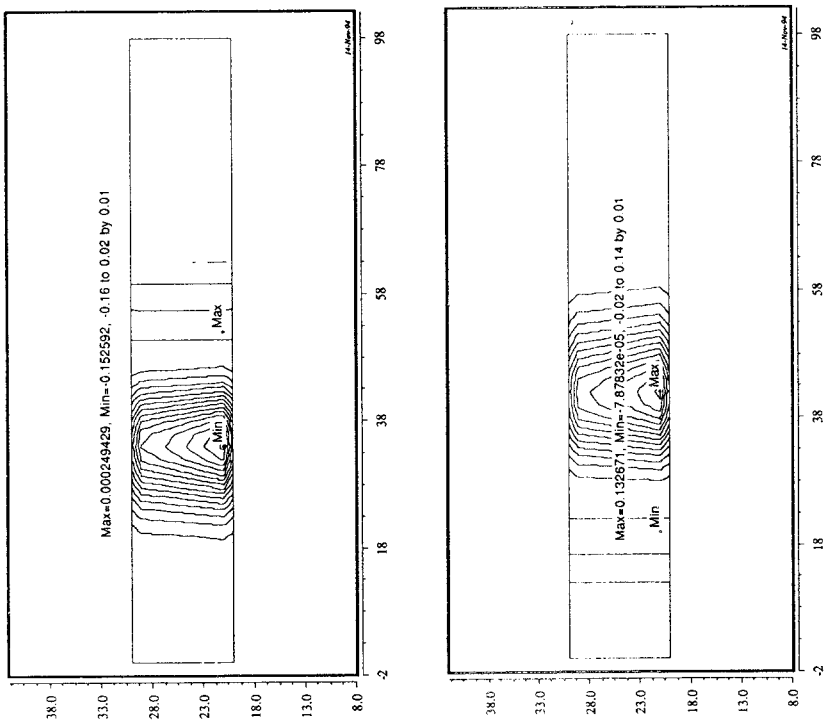

Fig. 8. Contours of the propagating radial E_r field. (Left) At computer time 200 (traveling downwards towards the surface). (Right) At time 280 (propagating upwards after reflecting off the surface).

the PSR0950+08 never 'turns off' as might be expected].

In the vicinity of the surface the B_θ magnetic insulation effect is lost and electrons accelerate across the line. During a 20 ms pulse duration, highly relativistic electrons can propagate as far as 6000 km and can modulate and slice the radiating current. Figure 11 depicts the electron flow in the scaled simulation. This flow is short-lived, lasting only as long as the negative potential is at the conductor surface. Figure 12 shows the associated current pulse. In contrast to the idealized cases shown in Figures 5b and 10b, the current in plasma is noisy and shows loss structure.

5 Pulsar Transmission Line Experiment

The pulsar magnetosphere was modelled with a 1 m long, pulse-power, coaxial transmission line. Electric energy in the form of a 1 ns, 2 MV/cm field was switched into the line. The geometry of the line was such that both ends, input and load, were terminated by conducting plates. The relative

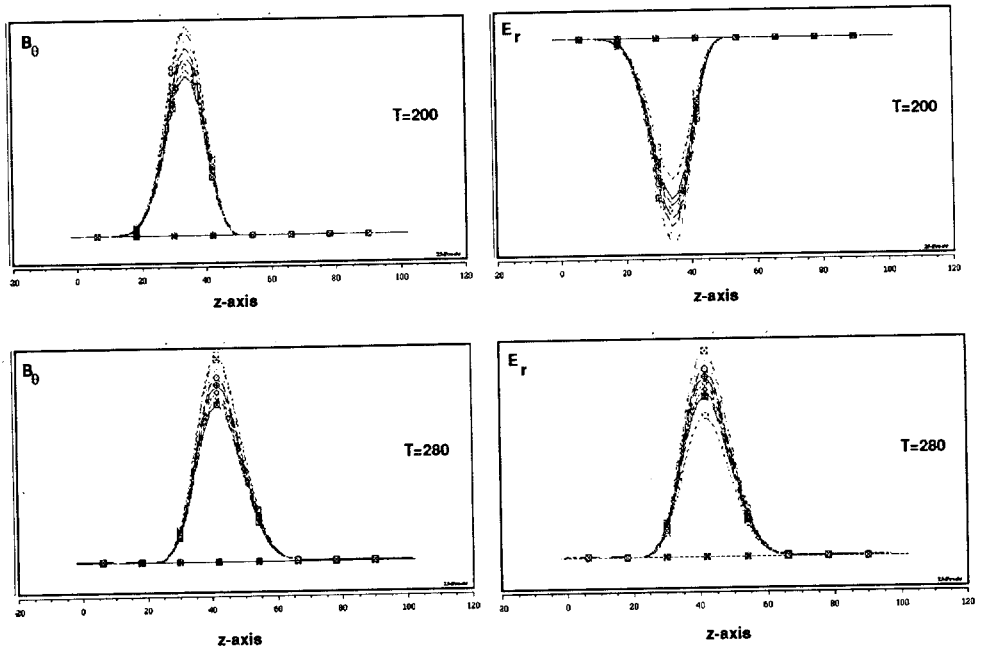

Fig. 9. (Top) Slices of B_θ and E_r at time 200. (Bottom) Slices of B_θ and E_r at time 280. The abscissa is in simulation spatial units.

permittivity of the dielectric medium was $\varepsilon = 1.998$. The pulse velocity is $v = c/\sqrt{\varepsilon} = 2.12 \times 10^8$ m/s.

The observed periodicity was 11.3 ns from voltage and current probes placed 20 cm from the input, as shown in Figure 13. For comparison, $i(t)$ and $v(t)$ from Eq.(1) are plotted on top of the data. While the calculated waveforms follow closely the observed waveforms, a number of differences

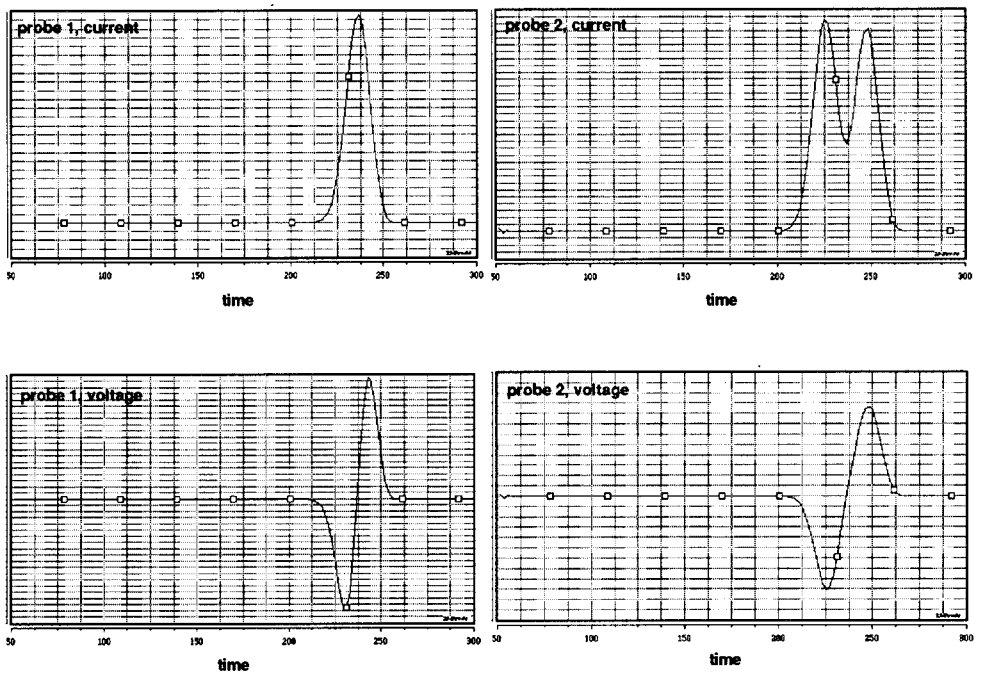

Fig. 10. Current and voltage pulses versus simulation time associated with E_r and B_θ of Figure 9. (Top) Current pulses at a probe located in the simulation region at (z, r, θ) locations (2,22,0) and (12,22,0), respectively. (Bottom) Voltage pulses at the same probe locations.

were noted. As mentioned, the entire line is a source of background radiation. Additionally, microstructure, noise, and low frequency drifts were seen on the observed data.

The experiment was instrumented with a number of x-ray detectors (XRD's) and the current waveform verifies relativistic transmission line currents as

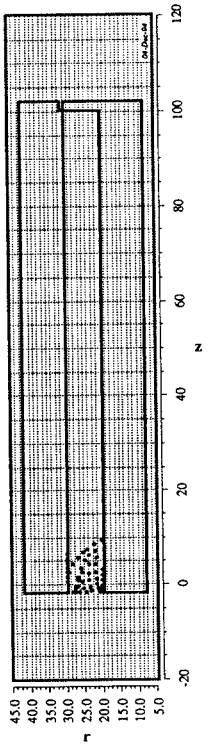

Fig. 11. Electrons flowing across the boundary near the pulsar surface at simulation time 240. The predominant flow is from the left to right boundary.

the source of the radiation observed. The voltage waveform verifies the linear polarization properties of the radiation and its 180° reversal over a pulse. Surprisingly, because of the relative shortness of the line, the detectors picked up radiation signals from both the input conducting plate and the short itself. While no probe was present at the short, the current waveform can be reconstructed and Figure 14 shows the current pulse-interpulse that might be expected from the 10^8 m magnetospheric transmission line, if the surface and disk terminating conductors are nearly parallel.

Because the currents at the surface/disk share the same polarity, if they are parallel, the radiation is in the same direction and both 'main' pulse and 'interpulse' components are observed. This phenomena can only occur for shorter lines; in a curved magnetosphere transmission line, the surface and disk currents may no longer be parallel and the high-γ radiation patterns will point in different directions.

It is signficant that the highly stressed line produced glitches when the magnetic insulation failed and electrical breakdown occurred. In all cases the glitches at high in the magnetosphere produce a line shortening and a

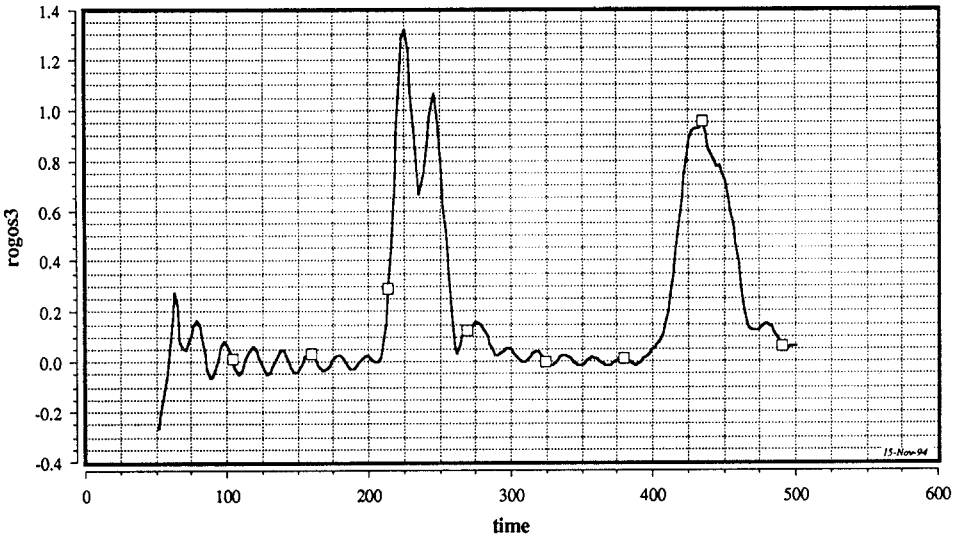

Fig. 12. Current pulses modified by the flow of electrons across the boundaries near the surface (Figure 11).

concomitant shortening in periodicity. This experimental observation is in agreement with pulsar observations.

6 Conclusions

VLA observations of the halo candidate pulsars PSR0809+74, PSR0942-13, and PSR0950+08 were made at 327.5 MHz. Each of these pulsars was observed in B Array (beamwidth of 15") in Phased Array Spectral Line mode for one hour. A very clean map of PSR0809+74 shows no evidence of a halo; maps of the other two pulsars are noiser and are the in process of further analysis.

On the theoretical side, our research involves the modeling of the global pulsar system, the pulsar magnetosphere, and the synchrotron radiation region, respectively. This paper reports only our magnetosphere transmission line simulations. We hope to publish the large scale and small scale simulations elsewhere. The models utilize transmission line equations and full three-dimensional, fully electromagnetic, particle-in-cell simulations to

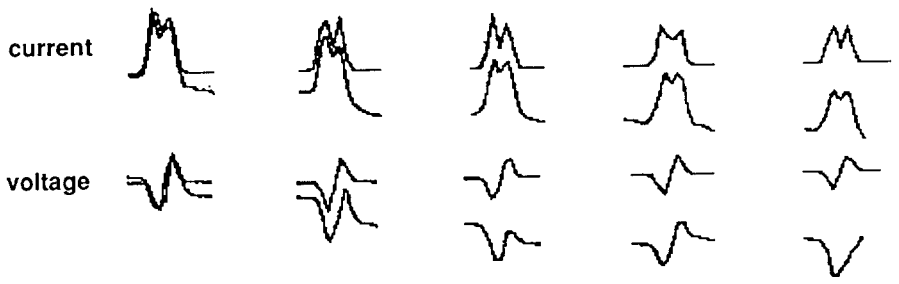

Fig. 13. Individual experimental current and voltage waveforms. The periodicity between waveforms is 11.3 ns. (Top) Current pulses. (Bottom) Voltage pulses. The calculated waveforms (upper waveforms) lie on a horizontal baseline while the measured waveforms lie on a downwards low-frequency component. The full-width-half-maximum duration of the pulses is about 5.3 ns.

determine pulse characteristics.

The simulated model produced a train of 10^{13-16} ampere pulses with periodicity 0.65 s. These $\gamma \sim 10^{7-10}$ currents are thought to be the source of the synchrotron radiation observed. The polarization properties of the model are consistent with observation: a high degree of linear polarization that changes 180 degrees over the pulse width, and circular or elliptical components. Whether or not the radiated pulse has a single or double pulse profile depends on the extent of the radiation region at the pulsar surface. If the radiating current is confined to a shallow region instead of an extended region, a single pulse profile will replace the double pulse. As shown below, this effect is frequency dependent: lower frequencies are associated with fields that are extended in the emission region and are more likely to show pulse structure. This is consistent with (Rankin) S_d class pulsars (Hankins & Rickett 1986).

The simulation results were verified with a high-voltage, transmission line

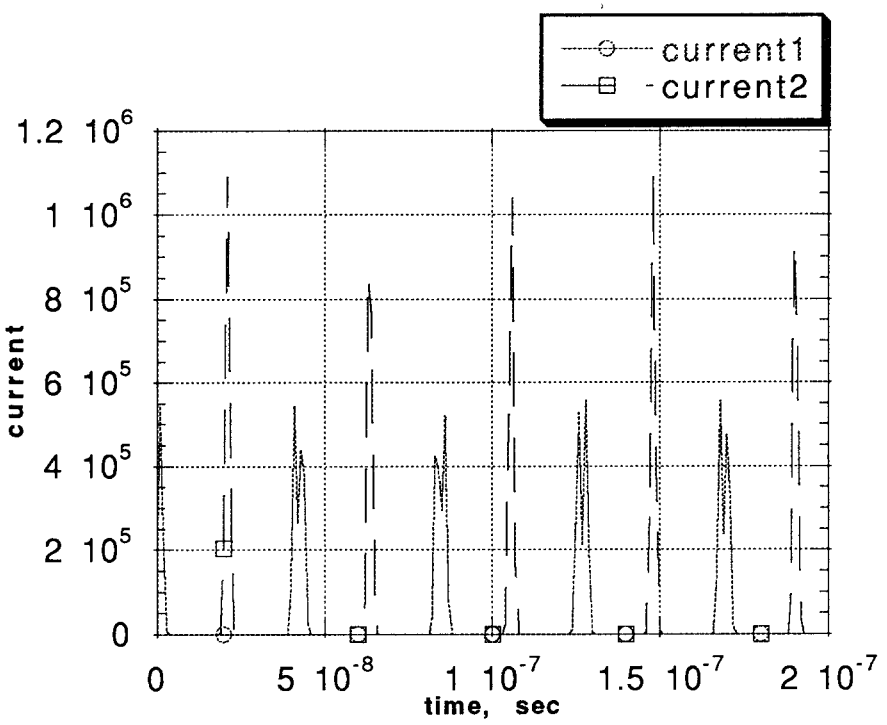

Fig. 14. Pulse and interpulses from the surface and disk locations.

experiment. Because of losses in the dielectric media and in synchrotron emission, the periodicity of the propagating pulses increases. However, the experiment dramatically showed that glitches, the flow of electron flux across the magnetosphere, can shorten the line and concomitantly the period.

The fractional frequency stability scaling versus measurement interval up to about 3×10^7 s ($\sim$ 1 year) for pulsars is nearly identical to that for trapped–ion clocks. This supports the pulsar surface–magnetosphere relativistic double layer model; itself a trapped-ion mechanism.

Both simulation and experiment suggest that micropulses and subpulses are produced particle–wave interactions in nonuniform plasma irradiated by an electromagnetic wave. This effect is produced when the magnetically insulated voltage pulse reaches the pulsar surface. Because of the curvature, magnetic insulation is lost, and plasma flows across this region. This tends to produce a resonating or modulation component on the the proper current pulse. We are currently investigating this phenomena with simulations of the emission region. If this effect is verified, then the source of the radiation energy may not be contained within the pulsar, but may instead derive from either the pulsar's interaction with its environment or by energy delivered

by an external circuit (Alfvén 1981)[2]. This hypothesis is consistent with both the long-term memory effect (provided either by the transmission line parameters or the double layer) of the time-averaged pulse and the occurance of nulling, when no subpulses are observed. As noted earlier, our results support the 'planetary magnetosphere' view (Michel 1982) where the extent of the magnetosphere, not emission points on a rotating surface, determines the pulsar emission. We are currently investigating this phenomena with simulations of the global environment.

7 Acknowledgements

One of the authors (KRH) thanks T. H. Hankins for advice on all past and ongoing parts of this project.

The other author (ALP) thanks Galen R. Gisler and Edward R. Harrison for suggesting the experimental approach to modeling pulsars.

The National Radio Astronomy Observatory is operated by Associated Universities, Inc., under cooperative agreement with the National Science Foundation.

References

Alfvén, H. : 1981 *Cosmic Plasma*, D. Reidel, Dordrecht, Holland

Backer, D. C. : 1988 "Pulsars", in *Galactic and Extragalactic Radio Astronomy*, G. L. Verschuur and K. I. Kellerman, eds., Springer–Verlag, New York, Chap. 11

Bietenholz, M. F., Frail, D. A., and Hankins, T. H. : 1991, "Does the Vela Pulsar have "Wisps"?", *ApJ*, **Vol. no. 376**, pp. L41–L44

Blandford, R. D., Ostriker, J. P., Pacini, F., and Rees, M. J. : 1973, "Radio Haloes around Old Pulsars — Ghost Supernova Remnants", *Astron. & Astrophys.*, **Vol. no. 23**, pp. 145–146

Burnell, J. B. : 1983 "The Discovery of Pulsars", in *Serendipitous Discoveries in Radio Astronomy*, K. Kellerman and B. Sheets, eds., National Radio Astronomy Observatory, Green Bank, West Virginia, pp. 160–170

Cordes, J. M., Romani, R. W., and Lundgren, S. C. : 1993 "The Guitar nebula: a bow shock from a slow–spin, high-velocity neutron star", *Nature*, **Vol. no. 362**, pp. 133–135

Frail, D. A., and Kulkarni, S.R. : 1991 "Unusual interaction of the high–velocity pulsar PSR1757−24 with the supernova remnant G5.4−1.2", *Nature*, **Vol. no. 352**, pp. 785–787

Glushak, A. P., Pynzar', A. V., and Udal'tsov, V. A. : 1981 "Pulsar Radio Haloes", *Sov. Astron.*, **Vol. no. 25(2)**, pp. 182–187

Gold, T. : 1968 *Nature*, **Vol. no. 218**, p. 731

Gopal–Krishna : 1978, "A ghost supernova remnant around PSR 0950+08", *MNRAS*, **Vol. no. 185**, pp. 521–525

Hester, J. J. : 1994 private communication

Jones, D. S. : 1964, *The Theory of Electromagnetism*, Macmillan, New York

Kennel, C. F., Fujimura, F. S., and Pellat, R. : 1979 "Pulsar Magnetospheres", *Space Science Reviews*, **Vol. no. 24**, pp. 407–436

[2] A double layer, set up by an electrostatic instability in a particle beam and fed from an external plasma source, seems to offer the long term P stability demanded by observation.

Kulkarni, S. R., and Hester, J. J. : 1988 "Discovery of a nebula around PSR1957+20", *Nature*, **Vol. no. 335**, pp. 801–803

Lysak, R. L.: 1993 "Generalized Model of the Ionospheric Resonant Cavity", in *Auroral Plasma Dynamics, Geophysical Monograph Series*, **Vol. no. 80**, R. L. Lysak, ed. (American Geophysical Union, Washington, DC), p.121

Michel, F. C. and Dessler, A. J. : 1981 *Astrophys. J.*, **Vol. no. 251**, pp. 654–664

Michel, F. C. : 1982 "Theory of the Pulsar Magnetospheres", *Rev. Mod. Phys.*, **Vol. no. 54**, pp. 1–66

Naik, P. K., and Kulkarni, V. H. : 1994 "Emission of Electromagntic Waves in Magnetized Plasma in the Presence of Field Aligned Currents", *Astrophys. Space Sci.*, **Vol. no. 218**, pp. 13–21

Peratt, A. L. : 1992a, *Physics of the Plasma Universe*, Springer-Verlag, New York. P.58

Peratt, A. L. : 1992b, *Ibid.*, Appendix A

Peratt, A. L. : 1992c, *Ibid.*, P.314

Peratt, A. L. : 1992d, *Ibid.*, Chap. 5

Thompson, B. & Lysak, R. L. : 1995 "The Effect of Static Electric Fields in the Alfvén Wave Model of Auroral Acceleration", *unpublished*

Verschuur, G. L. and Kellermann, K. I. : 1988, *Galactic and Extragalactic Radio Astronomy*, Springer-Verlag, New York.

Weiler, K. W., Goss, W. M., and Schwarz, U. J. : 1974, "A Search for Supernova Remnants in the Vicinity of Pulsars", *Astron. & Astrophys.*, **Vol. no. 35**, pp. 473–477